

# Deep Learning–Based Fixation Type Prediction for Quality Assurance in Digital Pathology

Oskar Thaeter<sup>1,2,3</sup>, Tanja Niedermair<sup>4</sup>, Jan E.G. Albin<sup>5</sup>, Johannes Raffler<sup>6,7</sup>, Ralf Huss<sup>8,9</sup>,  
and Peter J. Schüffler<sup>1,2,3,10</sup>

<sup>1</sup>Institute of Pathology, Technical University of Munich, Germany

<sup>2</sup>School of Computation, Information and Technology, Technical University of Munich, Germany

<sup>3</sup>Munich Center for Machine Learning, Germany

<sup>4</sup>Institute of Pathology, University of Regensburg, Regensburg, Germany

<sup>5</sup>Institute of Pathology, Medical Faculty Mannheim, University Heidelberg, Germany

<sup>6</sup>Digital Medicine, University Hospital of Augsburg, Germany

<sup>7</sup>Bavarian Cancer Research Center (BZKF), Augsburg, Germany

<sup>8</sup>Institute of Pathology and Molecular Diagnostics, University Hospital of Augsburg, Germany

<sup>9</sup>Current address: Bio<sup>M</sup> Biotech Cluster Development GmbH, Martinsried, Germany

<sup>10</sup>Munich Data Science Institute, Technical University of Munich, Germany

## Abstract

Accurate annotation of fixation type is a critical step in slide preparation for pathology laboratories. However, this manual process is prone to errors, impacting downstream analyses and diagnostic accuracy. Existing methods for verifying formalin-fixed, paraffin-embedded (FFPE), and frozen section (FS) fixation types typically require full-resolution whole-slide images (WSIs), limiting scalability for high-throughput quality control.

We propose a deep-learning model to predict fixation types using low-resolution, pre-scan thumbnail images. The model was trained on WSIs from the TUM Institute of Pathology (n=1,200, Leica GT450DX) and evaluated on a class-balanced subset of The Cancer Genome Atlas dataset (TCGA, n=8,800, Leica AT2), as well as on class-balanced datasets from Augsburg (n=695 [392 FFPE, 303 FS], Philips UFS) and Regensburg (n=202, 3DHISTECH P1000).

Our model achieves an AUROC of 0.88 on TCGA, outperforming comparable pre-scan methods by 4.8%. It also achieves AUROCs of 0.72 on Regensburg and Augsburg slides, pointing to scanner-induced domain shift as an open challenge. Furthermore, the model processes each slide in 21 ms, 400× faster than existing high-magnification, full-resolution methods, enabling rapid, high-throughput processing.

This approach provides an efficient solution for detecting labelling errors without relying on high-magnification scans, offering a valuable tool for quality control in high-throughput pathology workflows. Future work will improve and evaluate the model’s generalisation to additional scanner types. Our findings suggest that this method can increase accuracy and efficiency in digital pathology workflows and may be extended to other low-resolution slide annotations.

## 1 Introduction

Digital pathology has transformed histopathological diagnostics by digitising glass slides into whole-slide images (WSIs), allowing computational analysis of tissue samples [1]. A critical step in slide preparation is the fixation of tissue, which preserves cellular structures for downstream examination. The two predominant fixation methods are formalin-fixed, paraffin-embedded (FFPE) processing, in which tissue is chemically fixed and embedded in paraffin wax [2, 3], and frozen section (FS)

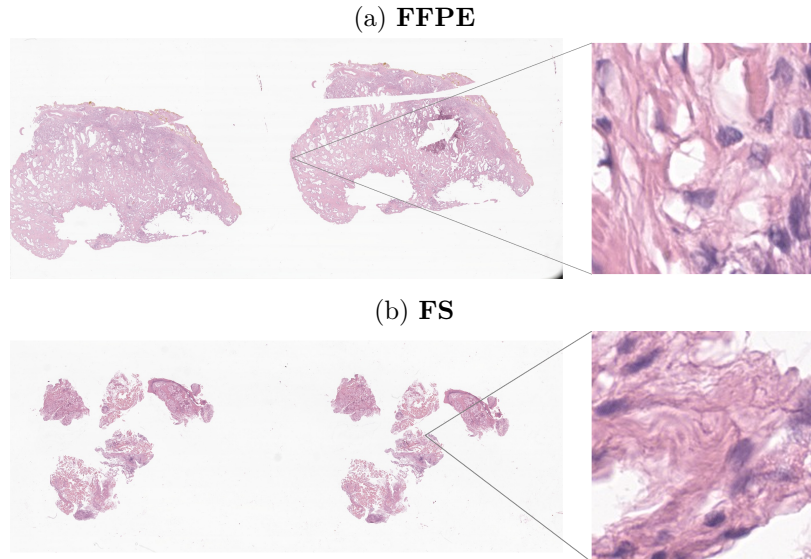


Figure 1: Example slides of FFPE and FS fixation types shown as thumbnails and at high magnification.

processing, in which tissue is snap-frozen for rapid intraoperative assessment [4] (Figure 3). Each method produces distinct histological characteristics: FFPE sections exhibit superior morphological preservation, while frozen sections, though faster to prepare, often contain freezing artefacts and less well-preserved cellular architecture (Figure 1).

Accurate fixation-type annotation is essential for reliable histopathological analysis. Jang et al. [5] showed that the performance of deep learning models for cancer diagnosis depends on the fixation type of the training data, which highlights the importance of correct annotations. In practice, mislabelling can occur when handling large volumes of slides, and retrospective correction across extensive physical or digital archives is costly and time-consuming.

Existing computational approaches to fixation-type classification operate on high-resolution WSIs. Dan et al. [6] achieved 98.91% accuracy using a VGG-19 model with majority voting over thousands of tiles extracted at  $40\times$  magnification, but this requires at least 10 seconds per slide. Such methods are impractical for high-throughput quality control or pre-scan verification, where the full-resolution image may not yet be available.

Most WSI file formats store a low-resolution thumbnail image, typically captured before the high-resolution scan and up to  $128\times$  smaller than the full image [7]. These thumbnails load orders of magnitude faster than the tiled pyramid of the full scan. If fixation type could be reliably predicted from these thumbnails alone, mislabelled slides could be flagged, re-annotated, or excluded before the high-resolution scan is even conducted, enabling efficient pre-scan quality control. Predicting fixation type at low magnification is difficult, however, because the cellular-level features that distinguish FFPE from FS sections are not resolved at thumbnail scale.

To our knowledge, the only prior work using thumbnail-level images for fixation-type prediction is that of Weng et al. [8], who employed a multi-modal, multi-task learning approach incorporating slide thumbnails, tile images, free text, and structured metadata. Their thumbnail-only model achieved an AUROC of 0.78, and their best model without high-magnification tiles reached 0.84, suggesting that fixation type is difficult to predict at the slide level alone.

In this work, we propose a deep learning model that predicts fixation type using only low-

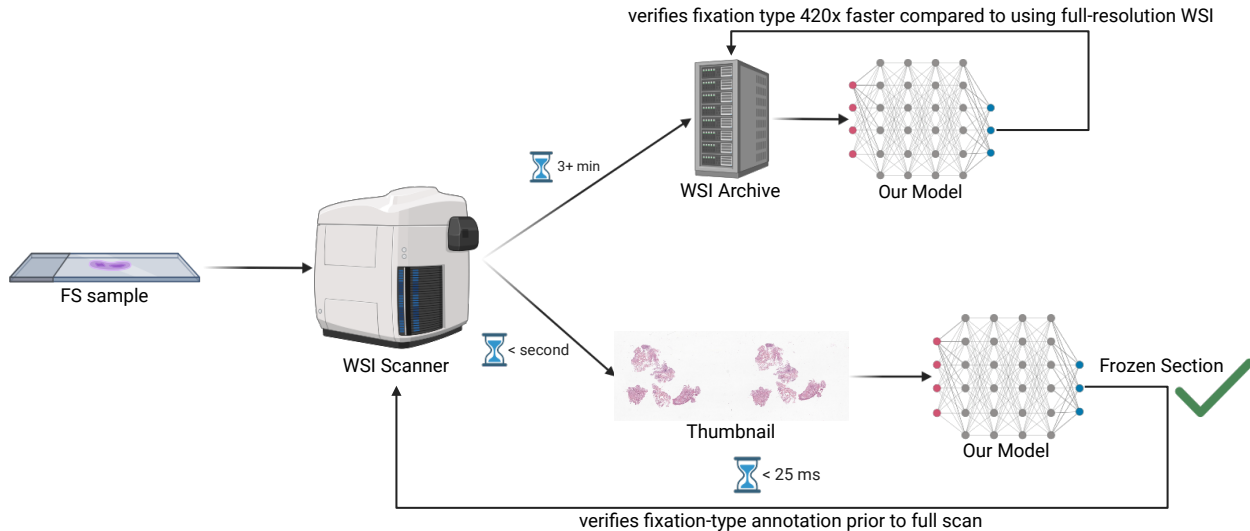


Figure 2: Possible applications of our approach in a digital pathology workflow. The fixation-type annotation can be verified before the high-resolution scan is conducted, allowing for re-annotation, re-examination, or skipping the scan entirely. Our approach can also be used as an efficient quality control measure in digital pathology archives.

*Created with BioRender.com*

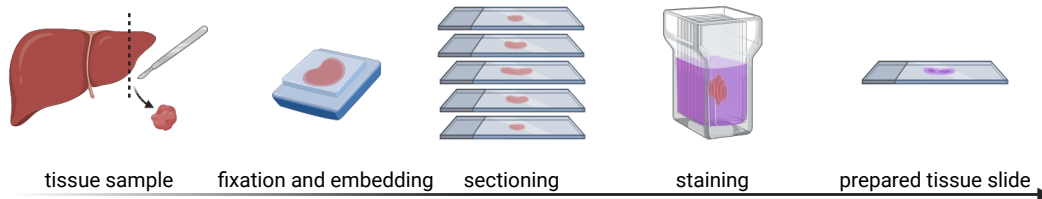
resolution pre-scan thumbnail images. We evaluate four pathology-pretrained vision transformer backbones and compare whole-slide and tiled-slide classification strategies. Trained on data from the TUM Institute of Pathology ( $n = 1,200$ , Leica GT450DX), our best model achieves an AUROC of 0.88 on a class-balanced subset of The Cancer Genome Atlas (TCGA,  $n = 8,800$ , Leica AT2), improving upon Weng et al.’s thumbnail-based result by 12.8%. The model processes each slide in 21 ms, which is  $400\times$  faster than high-magnification methods, making it suitable for high-throughput pre-scan quality control. We further evaluate cross-scanner generalisation on datasets from Augsburg (Philips UFS) and Regensburg (3DHISTECH P1000), identifying scanner-induced domain shift as a key challenge for future work. Figure 2 illustrates the envisioned application of our approach.

## 2 Related Work

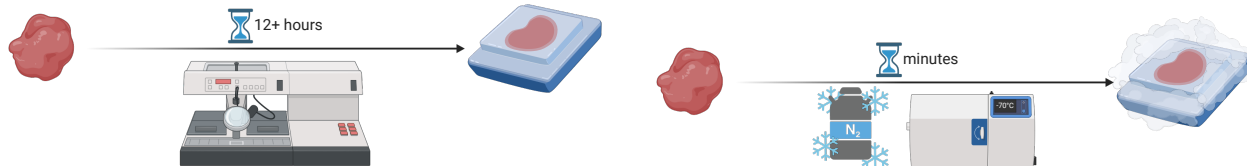
Computational quality control in digital pathology has primarily targeted scan-level artefacts rather than annotation correctness. Campanella et al. [9] developed a high-throughput blur detection system, and Haghighat et al. [10] proposed an automatic quality assessment pipeline producing focus and H&E staining quality scores for large-scale histology cohorts. These methods address image quality but do not verify slide-level metadata such as fixation type.

Fixation-type classification has received comparatively little attention. Dan et al. [6] fine-tuned a VGG-19 model on thousands of tiles per slide at  $40\times$  magnification, aggregating predictions via majority voting to achieve 98.91% accuracy. While highly accurate, this approach requires the full-resolution scan and takes at least 10 seconds per slide, precluding pre-scan use.

Weng et al. [8] addressed slide-level metadata prediction, including fixation type, through a multi-modal, multi-task framework combining a  $0.3125\times$  slide thumbnail ( $512 \times 512$  px), three tile images at  $5\times$  magnification ( $299 \times 299$  px), free text, and structured case-level data. Using ResNet-50 for image representation, they found that fixation type was difficult to predict from the slide thumbnail alone (AUROC 0.78) but considerably easier with high-magnification tiles,



(a) Overview of the tissue processing workflow.



(b) Formalin-fixed, paraffin-embedded (FFPE) process.

(c) Frozen section (FS) process.

Figure 3: Tissue processing workflow and the two fixation methods used in this study. (a) Tissue samples are fixed, sectioned, mounted, and stained. (b) In FFPE processing, tissue is formalin-fixed and paraffin-embedded before microtome sectioning. (c) In FS processing, tissue is snap-frozen and sectioned in a cryostat.

Created with BioRender.com

Table 1: Data splits of each dataset (FFPE, FS).

Dataset	Total	Train	Validation	Test
TUM	1080, 1080	600, 600	240, 240	240, 240
TCGA	4400, 4400	—	—	4400, 4400
Augsburg	392, 303	—	—	392, 303
Regensburg	101, 101	—	—	101, 101

attributing this to the loss of intracellular matrix detail in frozen sections at low resolution. Their work represents the only prior attempt at thumbnail-level fixation-type prediction and serves as our primary benchmark (Section 5.1).

## 3 Methods

### 3.1 Datasets

We used four datasets spanning different scanners and institutions (Table 1). The primary training dataset was obtained from the Institute of Pathology at the Technical University of Munich (TUM), comprising 2,160 class-balanced WSIs scanned on a Leica GT450DX. Three external datasets served as held-out test sets: a class-balanced subset of The Cancer Genome Atlas (TCGA,  $n = 8,800$ , Leica AT2), slides from Augsburg ( $n = 695$ , Philips UFS), and slides from Regensburg ( $n = 202$ , 3DHISTECH P1000). A portion of the TCGA data was discarded due to missing or corrupted images and to balance the classes.

FFPE thumbnail examples from each external dataset, alongside magnified regions at full resolution, are shown in Figure 6 (Appendix).

### 3.2 Pre-Processing

Using the OpenSlide library [7], we extracted a thumbnail from each WSI: either the auxiliary thumbnail image stored in the file or, if unavailable, the lowest pyramid level resized so that its longest side is 1,920 px. All thumbnails were oriented so that the width exceeded the height and stretched to a common size of  $896 \times 1,792$  px. Depending on the desired resolution, the images were then resized to one of four scales (Table 2) and divided into a grid of non-overlapping  $224 \times 224$  px tiles (Figure 4). The complete workflow is illustrated in Figure 5 for the M configuration.

Table 2: Thumbnail resolutions and corresponding tile grid configurations.

Name	Height $\times$ Width (px)	Grid (rows $\times$ cols)
XS	$224 \times 224$	$1 \times 1$
S	$224 \times 448$	$1 \times 2$
M	$448 \times 896$	$2 \times 4$
L	$896 \times 1792$	$4 \times 8$

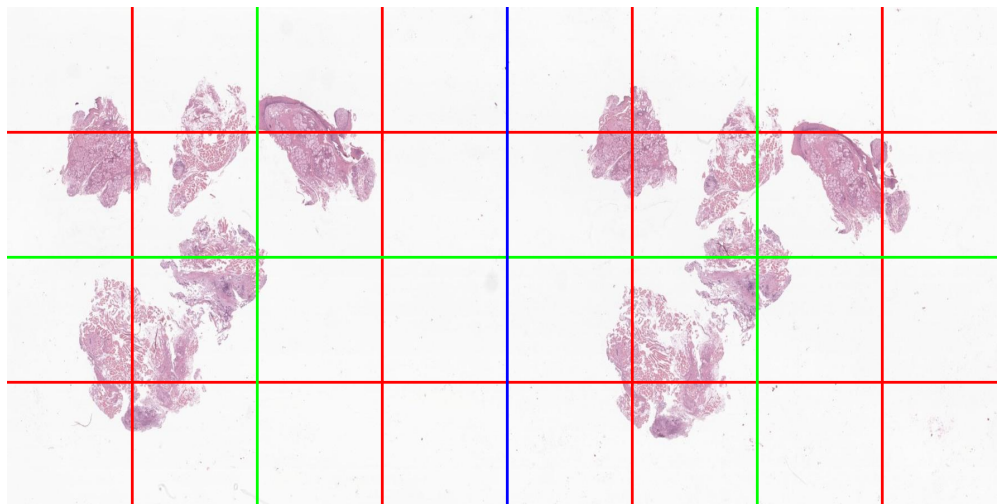


Figure 4: Stretched slide thumbnail with tile grids overlaid. Red: L grid ( $4 \times 8$ ), green: M grid ( $2 \times 4$ ), blue: S grid ( $1 \times 2$ ).

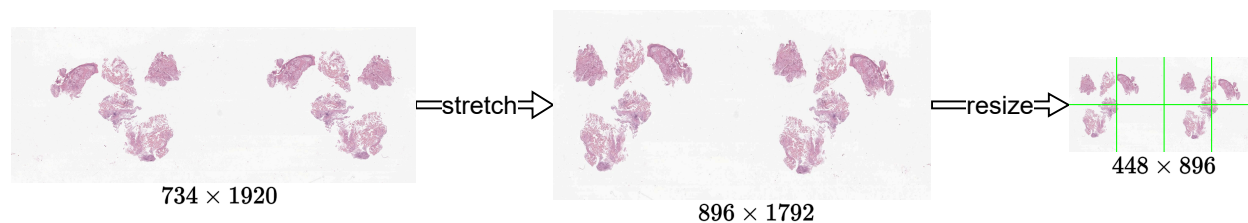


Figure 5: Pre-processing workflow for the M configuration. The thumbnail is stretched to  $896 \times 1,792$  px, resized to  $448 \times 896$  px, and divided into a  $2 \times 4$  grid of  $224 \times 224$  px tiles (green).

### 3.3 Vision Backbones

We compare four pathology-pretrained vision transformers as feature extractors (Table 3): TransPath [11] (ViT-S/16, pretrained on PAIP and TCGA via MoCo v3 [12]), UNI [13] (ViT-L/16, trained on 100M private images that do not include TCGA, avoiding data contamination), Virchow2 [14] (ViT-H/14, trained with DINOv2 [15] on 3.1M WSIs from Memorial Sloan Kettering), and H-Optimus-0 [16] (ViT-g/14, trained with iBOT [17]/DINOv2 on over 500K H&E WSIs, using register tokens [18]).

Table 3: Overview of the vision transformer backbones evaluated in this study.

Name	Architecture	#M Parameters	Embedding	Output
TransPath	ViT-S/16	22	384	class token
UNI	ViT-L/16	303	1024	
Virchow2	ViT-H/14	631	1280	class + mean patch token
H-Optimus-0	ViT-g/14	1100	1536	

### 3.4 Classification Approaches

We evaluate two families of approaches for slide-level fixation-type prediction from thumbnail images.

#### 3.4.1 Whole-Slide Classification

In the simplest variant, “**XS Slides**”, the thumbnail is resized to  $224 \times 224$  px and the entire backbone is fine-tuned end-to-end. Alternatively, in “**ViT Upscaling**”, we interpolate the position embeddings to accommodate the larger token count of an M-sized ( $448 \times 896$  px) thumbnail, preserving pretrained weights while fine-tuning only the attention and position embedding layers [19].

#### 3.4.2 Tiled-Slide Classification

This approach tiles the thumbnail into  $224 \times 224$  px patches processed independently by the backbone. We compared M (8 tiles) and L (32 tiles) configurations and found more tiles to be generally beneficial; we therefore used L ( $4 \times 8 = 32$  tiles). To obtain a slide-level prediction, we evaluated three aggregation strategies:

- **Soft voting**: averages tile-level sigmoid predictions, preserving differentiability for end-to-end training.
- **Multi-head attention**: computes attention weights  $\alpha_i$  over tile-level feature vectors  $\mathbf{f}_i \in \mathbb{R}^D$  and returns the weighted sum  $\mathbf{F}_{\text{att}} = \sum_{i=1}^n \alpha_i \mathbf{f}_i$ .
- **Transformer**: treats tile features as tokens with learned position embeddings; the class token is used for classification.

### 3.5 Classification Head

All approaches use a three-layer feed-forward classification head with batch normalisation [20], ReLU activations, and dropout ( $p = 0.1$ ) [21]:

$$\text{HiddenLayer}(x; W, b) = \text{Dropout}(\text{ReLU}(\text{BatchNorm}(\mathbf{W}x + b)))$$

The final layer outputs a single logit passed through a sigmoid function. Layer sizes for each backbone (Table 4) were selected via Bayesian hyperparameter optimisation using a Tree-structured Parzen Estimator [22] with Hyperband pruning [23] over 256 trials per backbone.

Table 4: Classification head layer sizes for each backbone, selected via hyperparameter optimisation.

Backbone	1st Layer	2nd Layer	3rd Layer
TransPath	2048	1920	128
UNI	1600	64	192
Virchow2	1728	64	192
H-Optimus-0	1856	192	128

## 4 Results

### 4.1 Model Selection

Table 5 reports the validation accuracy on the TUM dataset for all backbone–approach combinations. Tiled-slide approaches consistently outperformed whole-slide approaches across all backbones, with soft voting yielding the highest average accuracy (87%). Among backbones, UNI achieved the best average accuracy (87%), closely followed by Virchow2 and H-Optimus-0. The best overall configuration was UNI with soft voting, reaching 89% validation accuracy.

Table 5: TUM validation accuracy across backbones and classification approaches.

	Whole-Slide		Tiled-Slide		
	XS Slides	ViT Upscaling	soft voting	multiattention	transformer
TransPath	0.83	0.85	0.87	0.88	0.87
UNI	0.85	0.86	0.89	0.87	0.88
Virchow2	0.86	0.88	0.88	0.87	0.86
H-Optimus-0	0.84	0.86	0.88	0.87	0.85

Table 6 shows the corresponding single-threaded inference latencies. Latency scales with both backbone size and input resolution: XS Slides is the fastest, ViT Upscaling approximately  $7\times$  slower, and tiled-slide approaches approximately  $12\times$  slower. The three tiled-slide aggregation strategies add negligible overhead relative to the backbone forward passes. For the selected UNI–soft voting model, inference takes 21 ms per slide.

### 4.2 External Evaluation

We evaluated the selected UNI–soft voting model on the held-out TUM test set and the three external datasets (Table 7). On TUM, the model achieved an accuracy of 89% and an AUROC of 0.94. Performance generalised well to the TCGA dataset (accuracy 81%, AUROC 0.88), which was scanned on a different Leica model. Performance dropped on slides from non-Leica scanners, however: accuracy fell to 56% on Augsburg (Philips) and 50% on Regensburg (3DHISTECH), with AUROCs of 0.72 for both, indicating a strong scanner-dependent domain shift.

Table 6: Single-threaded inference latency (ms) across backbones and approaches.

	Whole-Slide		Tiled-Slide		
	XS Slides	ViT Upscaling	soft voting	multiattention	transformer
TransPath	0.88	4.15	4.26	4.31	4.67
UNI	2.37	15.23	20.87	20.95	21.85
Virchow2	4.28	34.91	56.49	56.63	57.74
H-Optimus-0	6.64	48.54	82.13	82.26	83.66

Table 7: Test results for the UNI–soft voting model on internal and external datasets.

Dataset	Scanner	Acc	F1	AUROC
TUM	Leica GT 450 DX	0.89	0.89	0.94
TCGA	Leica AT2	0.81	0.83	0.88
Augsburg	Philips UFS	0.56	0.65	0.72
Regensburg	3DHISTECH P1000	0.50	0.66	0.72

## 5 Discussion

### 5.1 Comparison to Prior Work

Our thumbnail-only model achieves an AUROC of 0.88 on TCGA, outperforming Weng et al.’s [8] single-task thumbnail-based model (0.78, +12.8%) and their best model without high-magnification tiles (0.84, +4.8%). It approaches their full multi-modal result (0.91), which relies on high-magnification patch images unavailable before scanning. Compared to Dan et al.’s [6] full-resolution approach (98.91% accuracy at 40 $\times$ ), our method trades 10 percentage points of accuracy for a 400 $\times$  reduction in inference time (21 ms vs.  $\sim$ 10s per slide), making it practical for pre-scan quality control where speed is essential.

These results confirm that pre-scan fixation-type classification from thumbnails is feasible and that the accuracy–efficiency tradeoff strongly favours low-resolution approaches for high-throughput workflows.

### 5.2 Limitations and Future Work

The main limitation of our approach is scanner-dependent domain shift. While the model generalises well across Leica scanners (TUM to TCGA), performance degrades on slides from Philips and 3DHISTECH devices (AUROC 0.72). This likely reflects differences in colour calibration, optics, and thumbnail generation across scanner manufacturers. Domain adaptation techniques, such as stain normalisation, scanner-aware training, or multi-site fine-tuning, could address this gap and should be explored in future work.

Beyond scanner generalisation, several directions merit investigation: incorporating additional pre-scan modalities (e.g., barcode metadata or macro images) to complement the thumbnail signal, extending the approach to other slide-level annotations such as staining method, and integrating explainability methods to support adoption in clinical practice.

## 6 Conclusion

We have presented a deep learning model for fixation-type classification that operates solely on low-resolution pre-scan thumbnail images. On the TCGA dataset, our approach achieves an AUROC of 0.88, improving upon the prior thumbnail-based state-of-the-art by 12.8%, while processing each slide in 21 ms. The primary remaining challenge is cross-scanner generalisation, which we have characterised through evaluation on three external datasets from different scanner manufacturers. Our results demonstrate that pre-scan thumbnail analysis is a viable and efficient quality control mechanism for high-throughput digital pathology and can serve as a starting point for broader pre-scan slide annotation verification.

## References

- [1] Liron Pantanowitz, Paul N. Valenstein, Andrew J. Evans, Keith J. Kaplan, John D. Pfeifer, David C. Wilbur, Laura C. Collins, and Terence J. Colgan. Review of the current state of whole slide imaging in pathology. *Journal of Pathology Informatics*, 2(1):36, 2011.
- [2] G. Bussolati. Fixation in histopathology: the mandate to renew. *Pathologica*, 114(4):275–277, 8 2022.
- [3] Cecil H Fox, Frank B Johnson, John Whiting, and Peter P Roller. Formaldehyde fixation. *Journal of Histochemistry & Cytochemistry*, 33(8):845–853, 1985.
- [4] J. Wallace. Frozen section overview, 2024. Accessed July 19, 2024.
- [5] Hyun-Jong Jang, In Hye Song, and Sung Hak Lee. Generalizability of deep learning system for the pathologic diagnosis of various cancers. *Applied Sciences*, 11(2), 2021.
- [6] L. Dan, J. Israel, S. R. Sarker, F. Stögbauer, W. Weichert, K. Steiger, and P. Schüffler. A machine learning approach to classify whole slide images by formalin-fixed paraffin-embedded or frozen section origin. Poster presented at 105. Jahrestagung der Deutschen Gesellschaft für Pathologie (DGP), 6 2022. Technical University of Munich, München, Germany.
- [7] Adam Goode, Benjamin Gilbert, Jan Harkes, Drazen Jukic, and Mahadev Satyanarayanan. Openslide: A vendor-neutral software foundation for digital pathology. *Journal of Pathology Informatics*, 4(1):27, 2013.
- [8] Wei-Hung Weng, Yuannan Cai, Angela Lin, Fraser Tan, and Po-Hsuan Cameron Chen. Multi-modal multitask representation learning for pathology biobank metadata prediction. *ArXiv*, abs/1909.07846, 2019.
- [9] Gabriele Campanella, Arjun Raj Rajanna, Lorraine Corsale, Peter J. Schüffler, Yukako Yagi, and Thomas J. Fuchs. Towards machine learned quality control: A benchmark for sharpness quantification in digital pathology. *Computerized medical imaging and graphics : the official journal of the Computerized Medical Imaging Society*, 65:142–151, 2017.
- [10] Maryam Haghghat, Lisa Browning, Korsuk Sirinukunwattana, Stefano Malacrino, Nasullah Khalid Alham, Richard Colling, Y. Cui, Emad A. Rakha, Freddy C Hamdy, Clare Verrill, and J. Rittscher. Pathprofiler: Automated quality assessment of retrospective histopathology whole-slide image cohorts by artificial intelligence, a case study for prostate cancer research. In *medRxiv*, 2021.

- [11] Xiyue Wang, Sen Yang, Jun Zhang, Minghui Wang, Jing Zhang, Junzhou Huang, Wei Yang, and Xiao Han. Transpath: Transformer-based self-supervised learning for histopathological image classification. In *International Conference on Medical Image Computing and Computer-Assisted Intervention*, pages 186–195. Springer, 2021.
- [12] Xinlei Chen\*, Saining Xie\*, and Kaiming He. An empirical study of training self-supervised vision transformers. *arXiv preprint arXiv:2104.02057*, 2021.
- [13] Richard J Chen, Tong Ding, Ming Y Lu, Drew FK Williamson, Guillaume Jaume, Bowen Chen, Andrew Zhang, Daniel Shao, Andrew H Song, Muhammad Shaban, et al. Towards a general-purpose foundation model for computational pathology. *Nature Medicine*, 2024.
- [14] Eric Zimmermann, Eugene Vorontsov, Julian Viret, Adam Casson, Michal Zelechowski, George Shaikovski, Neil Tenenholtz, James Hall, Thomas J Fuchs, Nicolò Fusi, Siqi Liu, and Kristen Severson. Virchow2: Scaling self-supervised mixed magnification models in pathology. *ArXiv*, abs/2408.00738, 2024.
- [15] Maxime Oquab, Timothée Darcet, Théo Moutakanni, Huy Q. Vo, Marc Szafraniec, Vasil Khalidov, Pierre Fernandez, Daniel Haziza, Francisco Massa, Alaaeldin El-Nouby, Mahmoud Assran, Nicolas Ballas, Wojciech Galuba, Russ Howes, Po-Yao (Bernie) Huang, Shang-Wen Li, Ishan Misra, Michael G. Rabbat, Vasu Sharma, Gabriel Synnaeve, Huijiao Xu, Hervé Jégou, Julien Mairal, Patrick Labatut, Armand Joulin, and Piotr Bojanowski. Dinov2: Learning robust visual features without supervision. *ArXiv*, abs/2304.07193, 2023.
- [16] Charlie Saillard, Rodolphe Jenatton, Felipe Llinares-López, Zeldá Mariet, David Cahané, Eric Durand, and Jean-Philippe Vert. H-optimus-0, 2024.
- [17] Jinghao Zhou, Chen Wei, Huiyu Wang, Wei Shen, Cihang Xie, Alan Loddon Yuille, and Tao Kong. ibot: Image bert pre-training with online tokenizer. *ArXiv*, abs/2111.07832, 2021.
- [18] Timothée Darcet, Maxime Oquab, Julien Mairal, and Piotr Bojanowski. Vision transformers need registers. *ArXiv*, abs/2309.16588, 2023.
- [19] Hugo Touvron, Matthieu Cord, Alaaeldin El-Nouby, Jakob Verbeek, and Hervé Jégou. Three things everyone should know about vision transformers. *ArXiv*, abs/2203.09795, 2022.
- [20] Sergey Ioffe and Christian Szegedy. Batch normalization: Accelerating deep network training by reducing internal covariate shift. *ArXiv*, abs/1502.03167, 2015.
- [21] Geoffrey E. Hinton, Nitish Srivastava, Alex Krizhevsky, Ilya Sutskever, and Ruslan Salakhutdinov. Improving neural networks by preventing co-adaptation of feature detectors. *ArXiv*, abs/1207.0580, 2012.
- [22] James Bergstra, Rémi Bardenet, Yoshua Bengio, and Balázs Kégl. Algorithms for hyperparameter optimization. In *Neural Information Processing Systems*, 2011.
- [23] Lisha Li, Kevin G. Jamieson, Giulia DeSalvo, Afshin Rostamizadeh, and Ameet Talwalkar. Hyperband: A novel bandit-based approach to hyperparameter optimization. *J. Mach. Learn. Res.*, 18:185:1–185:52, 2016.

## A Dataset Examples

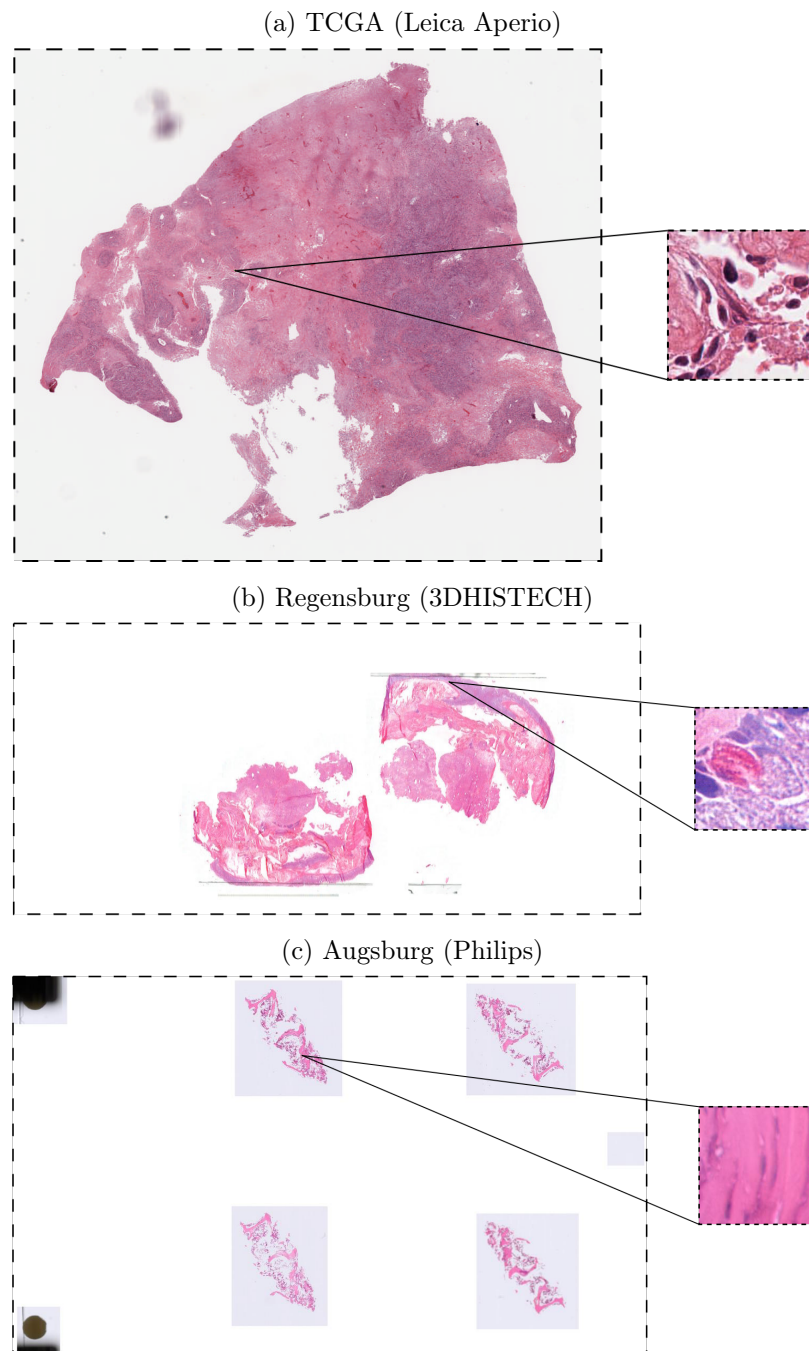


Figure 6: Thumbnail examples from different scanners with magnified  $224 \times 224$  px regions at full resolution.